PRIMER

Measuring forces and stresses *in situ* in living tissues

Kaoru Sugimura[1,2,*], Pierre-François Lenne[3,*] and François Graner[4,*]

ABSTRACT

Development, homeostasis and regeneration of tissues result from a complex combination of genetics and mechanics, and progresses in the former have been quicker than in the latter. Measurements of *in situ* forces and stresses appear to be increasingly important to delineate the role of mechanics in development. We review here several emerging techniques: contact manipulation, manipulation using light, visual sensors, and non-mechanical observation techniques. We compare their fields of applications, their advantages and limitations, and their validations. These techniques complement measurements of deformations and of mechanical properties. We argue that such approaches could have a significant impact on our understanding of the development of living tissues in the near future.

KEY WORDS: Mechanics, Morphogenesis, Quantitative biology

Introduction

During morphogenesis, developmental processes are based on coordinated changes in cell size, shape and position over time. These are under the regulation of both genetics and mechanics. Genetic information is translated into biochemical signals, which regulate body axis specification, tissue patterning, and the sequence and timing of cell activities such as proliferation, migration and differentiation. Mechanics provides another layer of regulation in development (Davidson et al., 2009), which could be as evolutionarily conserved as genetic regulation (Savin et al., 2011).

Mechanical forces and stresses (see Box 1) arise at the molecular level in part from the distribution and regulation of molecular motors (Young et al., 1991; Bertet et al., 2004; Lecuit et al., 2011). Cells integrate these forces to pull and push on their neighbors and ultimately deform tissues, depending on cell and tissue material properties (Heisenberg and Bellaïche, 2013; Sampathkumar et al., 2014). Different forces and levels of stiffness also control transcriptional programs involved in cell differentiation (Farge, 2003; Kahn et al., 2009; Mammoto et al., 2012), especially in organs with a mechanical role, such as bones, muscles, heart or blood vessels. Forces determine cellular behaviors during tissue repair and homeostasis (Guillot and Lecuit, 2013). Understanding force generation and sensing, feedback, and how these mechanics integrate with genetic inputs in multicellular tissues is an active field of research that should help us achieve a comprehensive and multi-scale picture of tissue and organ development, homeostasis, regeneration and disease (Davidson et al., 2009).

[1]Institute for Integrated Cell-Material Sciences (WPI-iCeMS), iCeMS Complex 2, Kyoto University, Yoshida Honmachi, Sakyo-ku, Kyoto 606-8501, Japan. [2]JST, PRESTO, 5 Sanban-cho, Chiyoda-ku, Tokyo 102-0075, Japan. [3]Institut de Biologie du Développement de Marseille, Aix-Marseille Université, CNRS UMR7288, Case 907, Parc Scientifique de Luminy, F-13288 Marseille Cedex 9, France. [4]Laboratoire Matière et Systèmes Complexes, Université Denis Diderot - Paris 7, CNRS UMR7057, 10 rue Alice Domon et Léonie Duquet, F-75205 Paris Cedex 13, France.

*Authors for correspondence (tissue.stress@univ-paris-diderot.fr)

Measurements of forces and stresses have up to now mainly been performed in cells in culture (Addae-Mensah and Wikswo, 2008; Kollmannsberger and Fabry, 2011). Recently, there is an increasing body of literature on methods (and applications thereof), either transferred from *in vitro* to *in vivo*, or specifically developed for *in vivo* applications. Here we review these techniques, which are either already, or likely soon to become, part of a versatile toolbox to study tissue mechanics *in vivo*, especially during development. We discuss methods that (ordered from the more direct to the less invasive) are based on contact manipulation, manipulation using light, visual sensors, and non-mechanical observation techniques. For each method, we explain the principle on which it relies, list the quantities it measures and over which range, discuss its advantages and drawbacks, and suggest examples of biological questions it can help to address *in vitro* or *in vivo*. Table 1 provides an overview of each method, including the cost involved in implementing it. With this Primer article, we hope to help newcomers in the field to select techniques suitable to their needs, to encourage the formation of a community with common cross-validation methods, and to improve the integration of experimental data into multi-scale models of cell and tissue mechanics.

Understanding the mechanics of morphogenesis requires integration of different types of measurements (Koehl, 1990). We review here the techniques that measure forces or mechanical stresses. It is important to recognize that most force measurements extract physical parameters using assumptions on the material properties, which must be validated experimentally. Note that we do not review two other types of techniques that are very important and for the most part already well established: those that measure, in the absence of mechanical manipulation, the deformation of cells and tissues or their change of deformation during development and those that measure the material mechanical properties, for instance how stiff or viscous the tissue is (Fung, 1993; Oates et al., 2009; Davidson et al., 2009; Labouesse, 2011).

Contact manipulation

In contact manipulation methods, a controlled force, either pushing or pulling, is applied to a cell or tissue sample by direct mechanical contact. Such approaches can be used on samples that are accessible to a probe, without a rigid external layer; their advantage is that they provide direct measurements of the applied force. When the sample deformation response mostly originates from internal forces and/or stresses, measuring the former enables one to infer the latter. For example, if the material behaves like a fluid, in particular in that it tends to minimize the surface area of its interface with a surrounding medium, one can determine the energy cost per unit area (also equivalent to force per unit length) associated with increasing this interface, commonly referred to as 'surface tension'.

Pushing

Contact manipulation tools that push on a sample, such as microplates or indenters (Davis, 1984; Davidson and Keller, 2007), provide information on mechanical properties (stiffness,

> **Box 1. Definition of mechanical terms**
>
> **Stress.** A coarse-grained description of the forces within a tissue. When a piece of tissue experiences a force from a neighboring tissue region (A), mechanical stress (σ) is defined as the ratio of the force (F) to the area of contact (A) with that region (B, top equation). Tension and compression correspond to forces pointing respectively outwards from and inwards to the body.
>
> **Deformation.** Deformation (also called 'strain') is the relative change in size of an object subjected to a force. In one dimension, it is a dimensionless number, ε (B, bottom equation): the fraction of change in the object length (where L is the new length and L_0 the original length), which would be positive for elongation or negative for contraction. In two (C) or three dimensions, elongation in one direction can coexist with contraction in another direction, or can occur in isolation, so that the deformation is described by amplitudes in different directions. Schematics show uniaxial extension (top); uniaxial compression (middle) (in both these cases, there is a change in total volume); and pure shear, or convergent extension (bottom), in which the body is compressed in one direction and extended in the orthogonal direction, while the volume remains constant. In this figure and others, thick outlined arrows indicate forces. Forces are expressed in Newtons (N), stresses in Newtons per square meter or Pascals (Pa).

$$\text{Stress } \sigma = \frac{F}{A}$$

$$\text{Deformation } \varepsilon = \frac{L - L_0}{L_0}$$
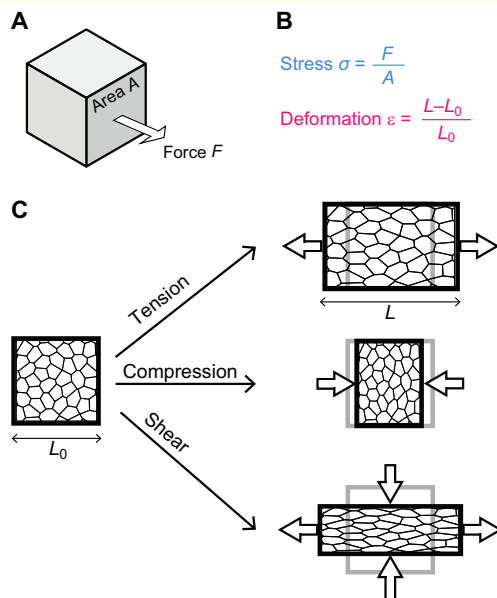
viscosity) but also on forces and stresses, in particular the material's surface tension and internal pressure at different spatial scales. Microplates are parallel plates that apply uniaxial compression on a large surface area of the sample; one of these plates, either soft itself or linked with a soft spring, acts as a force transducer. The sample surface tension can then be inferred from the applied pressure and the profile shape of a single cell or aggregate (Fig. 1Aa). Surface tensions between tens of µN/m and tens of mN/m have been measured *in vitro* on cell aggregates (Norotte et al., 2008; Mgharbel et al., 2009) or soft embryonic tissues. Because tissue surface tension impacts on phenomena such as cell mixing, sorting and spreading, these measurements can help predict possible outcomes of experimental investigation and give insights into these behaviors during development (Foty et al., 1994, 1996; Fig. 1Ab).

Indenters push on the sample across a small contact area rather than the whole tissue (Lomakina et al., 2004; Fig. 1Ba). A variety of indenters can be used, covering six orders of magnitude in terms of forces they can apply, from nanometer indenters [atomic force

microscopy (AFM)] for pN to nN, to micrometer indenters (often rod shaped) for µN. For example, AFM has been used in cells dissociated from the early zebrafish embryo to measure surface tension and infer the contractility of the cell cortex (Krieg et al., 2008). This study provided evidence that differential tension functions to sort ectoderm, mesoderm and endoderm progenitor cells, leading to germ-layer organization of the zebrafish embryo.

In plants, the cell wall resistance to deformation is due to its mechanical properties but also partly due to the cell internal turgor pressure (force per unit area), which can be distinguished and measured *in vivo* (Forouzesh et al., 2013; Beauzamy et al., 2015; Fig. 1Bb). Analyzing developmental changes in turgor pressure using AFM showed that these can be finely tuned to support flower opening, anther dehiscence and lateral root emergence (Beauzamy et al., 2014).

Pulling

Micromanipulators that pull on a cell or tissue sample deform it by aspirating it through the aperture of a pipette with circular or rectangular cross-section. At equilibrium, the shape of the sample part inserted into the pipette entrance results from the balance of its surface tension and the pressure of aspiration (Evans and Yeung, 1989; Tinevez et al., 2009). The sample surface tension can then be inferred from the applied aspiration pressure and the radii of the sample inside and outside the pipette (Fig. 1Ca).

Such surface tension measurements provide absolute values with precision of a few percent: on cell aggregates *in vitro*, the biological variability dominates the experimental uncertainty (Guevorkian et al., 2010). These experiments require a few minutes and are therefore suitable for morphogenetic events much slower than minutes, but not for quicker processes.

In one key example in the living mouse embryo, a quantitative map in space and time of each cell surface tension using pipette aspiration revealed that the first morphogenetic movement of the embryo, compaction, is mediated by increased actomyosin contractility, rather than by increased cell-cell adhesion as commonly thought (Maître et al., 2015; Fig. 1Cb). Pipette aspiration has also been used at larger scales to measure the surface tension of a group of sea urchin cells (Mitchison and Swann, 1954) and of mouse eggs (Larson et al., 2010), and to uncover the role of tissue tension to ensure vertebrate 3D body shape (Porazinski et al., 2015).

Manipulation using light

In epithelia, cell-cell contacts are often supported by adherens junctions, which can be considered as one-dimensional structures. Tension at adherens junctions is in this case a line tension (expressed in Newtons). To measure this tension, two methods use light to perturb the cell-cell junction: optical tweezers and laser ablation; the latter can also be applied at tissue scales to measure stresses. Thanks to the penetration of light, both methods can be applied within the living organism.

Optical tweezers

Optical tweezers use gradients of light intensity to manipulate injected particles within cells (Svoboda and Block, 1994). A transparent particle (with a higher refraction index than its surrounding medium) in a focused laser beam is subject to a gradient force pulling it towards the high intensity region (focus) of the beam (Fig. 2Aa), while a scattering force pushes it away from the focus along the direction of light propagation (Fig. 2Ab). When the gradient forces dominate over the scattering forces, an effective

Table 1. Comparison of the methods discussed

	Measured quantities	Measurable range	Time scale*	Size scale‡	Advantages	Disadvantages	Cost
Indentation/ microplates/ AFM	Cell or aggregate surface tension	0.1 Pa	s-h	1-100 µm	Absolute measurements	Contact method	€€-€€€€
Pipette aspiration	Cell or aggregate surface tension	µN/m-mN/m	>10 s	1-100 µm	Absolute measurements	Contact method	€€
Optical/magnetic tweezers	Cell junction tension	pN-nN	ms-min	0.1-10 µm	Non-contact; absolute measurements	Delicate calibration	€€€
Subcellular laser ablation	Cell junction tension to viscous drag ratio	NA	0.1 s-min	0.1-10 µm	Non-contact	Possible collateral damage	€€-€€€
Tissue-scale laser ablation	Tissue stress to viscosity ratio	NA	s-min	10 µm-1 mm	Non-contact	Requires sample and laser alignment; few experiments per sample	€€-€€€
FRET force probe	Intramolecular tension	pN	Video rate	nm	Molecular measurements	Requires different control constructs; delicate calibration	€
Liquid drops	Cell-scale stress	~0.1-60 kPa	0.1 s-h	>5 µm	Absolute measurements	Requires surface chemistry of droplets	€€
Birefringence	Tissue-scale stress	>10 kPa	Video rate	>µm	Global	Requires flat, transparent sample; delicate calibration	€
Force inference	Relative cell junction tension, cell pressure	NA	Video rate	>µm	Image based; global	Requires image segmentation	€

*Time scale of the mechanical processes that can be probed.
‡Size scale of the mechanical processes or mechanical elements that can be probed.
NA, not applicable because only relative measurements.
Cost excluding the microscopes: € (<€10,000); €€ (€10,000-50,000); €€€ (€50,000-100,000); €€€€ (€100,000-200,000).

optical trap is created; its strength depends on the geometry and refraction index of the particle, as well as of the intensity profile of the laser beam. Optical tweezers can be combined with most microscope setups, whereby the infrared laser used to produce the laser trap is focused by the same objective lens as the one used for image collection.

Forces applied to the transparent particle, usually a bead, can be used to counterbalance (and thus measure) subcellular forces. The tissue regions accessible to this method are limited by the need to inject transparent beads within the sample, and by the depth of sample penetration by light. Measurements are quantitative provided *in situ* calibration is possible, which can be challenging in living tissues. If beads can be introduced inside cells, for instance by injecting them in the *Drosophila* embryo syncytium just before cellularization (Bambardekar et al., 2015), they can be individually manipulated and used to push against and deform cell junctions. Measurable forces are typically on the order of 1-100 pN, which could be suitable for cell junction tensions.

In some cases, subcellular structures such as the nucleus or membranes can be trapped directly, and the method becomes non-invasive. For instance, in the early *Drosophila* embryo, direct trapping of a cell-cell junction *in vivo* (Fig. 2Ac) can be achieved. Such a direct method showed that cell-cell junction tension is in the order of 100 pN and that tension equilibrates over a few seconds (a short timescale compared with the contractile events that drive morphogenetic movements), and delineated how subcellular deformations propagate in the tissue plane (Bambardekar et al., 2015).

Note that a variant of optical tweezers is magnetic tweezers, which trap injected magnetic particles through gradients of magnetic field (Tanase et al., 2007). The method measures forces

in the order of pN to nN. Magnetic tweezers have been used to apply and/or measure forces and stresses. For instance, *in vitro*, surface tension of aggregates has been measured and even modified using magnetic manipulation (Mazuel et al., 2015). *In vivo*, by implantation of a magnet in the mouse colon, ultra-magnetic liposomes, which are stabilized in mesenchymal cells, were manipulated to impose compression on surrounding epithelial tissues and mimic endogenous early tumor growth stress (in the order of 1200 Pa) (Fernández-Sánchez et al., 2015). Again, a limiting step is the need to inject beads; the primary advantage is that a well-controlled, calibrated, quickly varying force can be flexibly applied even deep into a sample.

Laser ablation
If a tissue is cut with a scalpel, the wound initially opens further, demonstrating that the tissue tension was positive before cutting (Beloussov et al., 1975). The use of a standard force sensor in such experiments can reveal the value of the tension [as has been done, for example, with bacterial biofilms, where such force sensors determined that biofilms are under compression rather than tension (Trejo et al., 2013)]. Cutting tissues with a scalpel is obviously only feasible at the macro scale; at smaller scales, lasers can be used.

In subcellular laser ablation (Ma et al., 2009), a tightly focused laser is targeted to a particular cellular structure to disrupt the biological structures that support force transmission: most commonly cell-cell junctions, but also cytoskeletal filaments. Severing these structures by laser ablation thus provokes a sudden force imbalance. Vertices at the extremities of the junction move apart, pulled by the tension of adjacent junctions (chapter 4 of Labouesse, 2011). Such movements can be visualized using fluorescent reporters for the structures of interest (Fig. 2Ba).
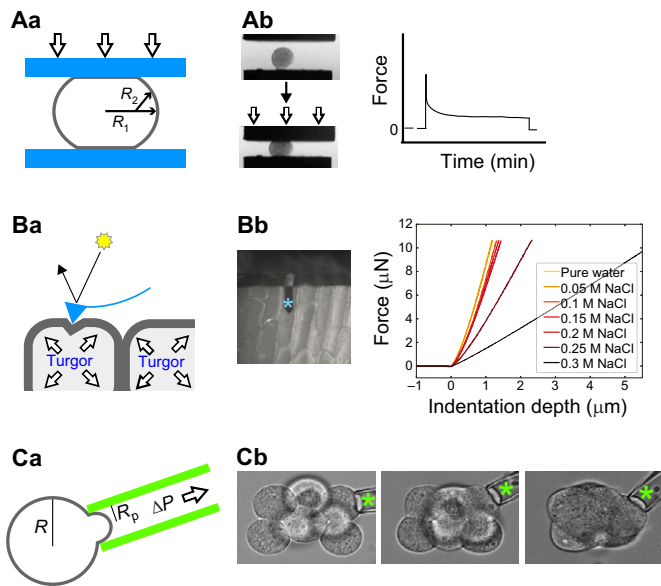
Fig. 1. Contact manipulation. (A) Pushing: microplates. (Aa) A force applied on a cell or aggregate sample compresses it with a known applied pressure (*P*). Image analysis determines the sample profile shape, which is characterized by the local mean curvature of the sample interface (*H*) (modified from Foty et al., 1996). Their ratio (according to the equation $P=\gamma H$) measures the sample surface tension (γ), which is its tendency to minimize the surface area of its free interface, expressed in Newtons per meter. Here, $H=1/R_1+1/R_2$ where R_1 and R_2 are called the 'two principal radii of curvature', in planes respectively perpendicular and parallel to the figure. See Norotte et al. (2008) and Mgharbel et al. (2009) for more complex and exact solutions used. (Ab) Deformation of an aggregate of chicken heart cells by microplates, allowing its surface tension to be measured. Force curve during measurement is illustrated on the right. (B) Pushing: Atomic force microscopy (AFM). (Ba) As the AFM cantilever tip (blue triangle) is pushing on the sample, either approaching or retracting from it, the cantilever shape changes (cantilever deflection). A laser beam (yellow star) is reflected on the AFM cantilever, and light deflection reveals cantilever deflection. The slope of the force-indentation curve yields an estimate of the turgor pressure. (Bb) Image shows an onion epidermis in water scanned by the AFM cantilever (asterisk). Graph shows examples of force-indentation curves for different concentrations of salt in the water. (C) Pulling: pipette aspiration. (Ca) Surface tension measurement by aspiration in a pipette, here with circular cross-section (modified from Guevorkian et al., 2010). During aspiration, the aspiration pressure is increased to above that of the external pressure (the pressure difference is ΔP). The surface tension (γ) of the cell or cell aggregate is then determined by measuring its radius in the pipette (R_p) and outside the pipette (*R*), according to the equation $\Delta P=2\gamma(1/R_p - 1/R)$. (Cb) Tension-mapping experiment in the early mouse embryo at three successive stages of compaction. Asterisks indicate the pipette. Adapted with permission from: (Ab) Foty et al. (1996), (Bb) Beauzamy et al. (2015) and (Cb) Maître et al. (2015).

The rate and degree of displacement can be used to determine the tension that existed before ablation in the targeted structures, such as cell-cell junction tension (Fig. 2Bb).

One potential complication is that the displacement of cell-cell junctions and vertices will also be affected by viscous drag on the cell-cell junction, which is hard to assess due to its dependence on the cell-cell junction geometry and cell viscosity. If one can assume that the viscous drag changes much less than the tension between compared conditions, this method yields relative force measurements. A major advantage is the possibility of quickly repeating the experiment at different positions in a tissue to accumulate statistics, e.g. on several cell-cell junctions. This technique is easily combined with different types of microscopes using simple optical elements and can be applied to a large

variety of tissues and organisms *in vivo*. Near-infrared femtosecond lasers like those used in multiphoton microscopes (Rauzi et al., 2008) or pulsed UV lasers (Farhadifar et al., 2007) can be employed.

In the *Drosophila* embryo and imaginal disc, cell-scale laser ablation experiments have revealed that cell contractility drives morphogenetic movements and determines cell geometry (Kiehart et al., 2000; Farhadifar et al., 2007), and that anisotropy of tension at cell junctions drives cell intercalation and tissue elongation (Fig. 2Ba; Rauzi et al., 2008). In the *Caenorhabditis elegans* single-cell embryo, anisotropy of cortical tension measured by laser ablation produces cortical flows, which establish antero-posterior polarity (Mayer et al., 2010).

Slightly enlarging the scale to probe the stress directly at the tissue level, a laser can simultaneously ablate a line of cells to generate a wound (Hutson et al., 2003; Behrndt et al., 2012; Campinho et al., 2013; Porazinski et al., 2015). The initial velocity of wound margin retraction or closure after ablation measures the stress-to-viscosity ratio within the tissue. Alternatively, severing a large circle (Bonnet et al., 2012; Etournay et al., 2015) reveals at once the main directions of stress and its anisotropy (Fig. 2Ca,Cb). Wound healing responses can trigger additional sources of tension, which can also be used to redirect tension or induce anisotropy within tissue tension field. In the zebrafish embryo, the redirected tension was used to demonstrate an effect of tissue tension on orientation of the spindle axis (Campinho et al., 2013).

Large-scale ablation offers the advantage of yielding coarse-grained stress measurements, which are relevant for tissue-scale mechanics. Its drawbacks are that it is a relative measurement unless the tissue viscosity is known, and that there are a number of technical conditions that must be respected. For example, the ablation time and the time between successive images should be short, typically less than a second (this is also crucial for subcellular ablation). If not, the velocity immediately after ablation cannot be properly measured (Ma et al., 2009). The maximal size of any ablation is determined by the three-dimensional curvature of the tissue, because all cells to be ablated should be in the same focal plane simultaneously. Efficient and well-controlled experiments require proper axial and lateral laser alignment.

In *Drosophila*, large-scale laser ablation revealed that dorsal closure is mechanically driven by the contractility of a supracellular actomyosin string and amnioserosa cells (Hutson et al., 2003). Such experiments also helped to understand how planar cell polarity can control mechanics during dorsal thorax morphogenesis (Bonnet et al., 2012), and how the wing morphogenesis is affected by tensions at its boundaries (Etournay et al., 2015).

Visual sensors
Visual sensor methods avoid deforming or disrupting the cell or tissue. FRET (Förster resonance energy transfer) tension sensors can be used to estimate subcellular forces at the molecular scale, and the use of liquid drops allows tissue stresses at the cellular scale to be probed.

FRET
Forces are produced, supported and transmitted by molecular elements such as cytoskeletal and adhesion components. FRET can be used to measure the amplitude of tension that these molecules experience in tissues. A FRET tension sensor module consists of two fluorophores: a donor and an acceptor (Miyawaki, 2011; Gayrard and Borghi, 2015; Fig. 3Aa). FRET efficiency (*E*) decreases sharply with the distance *R* between fluorophores
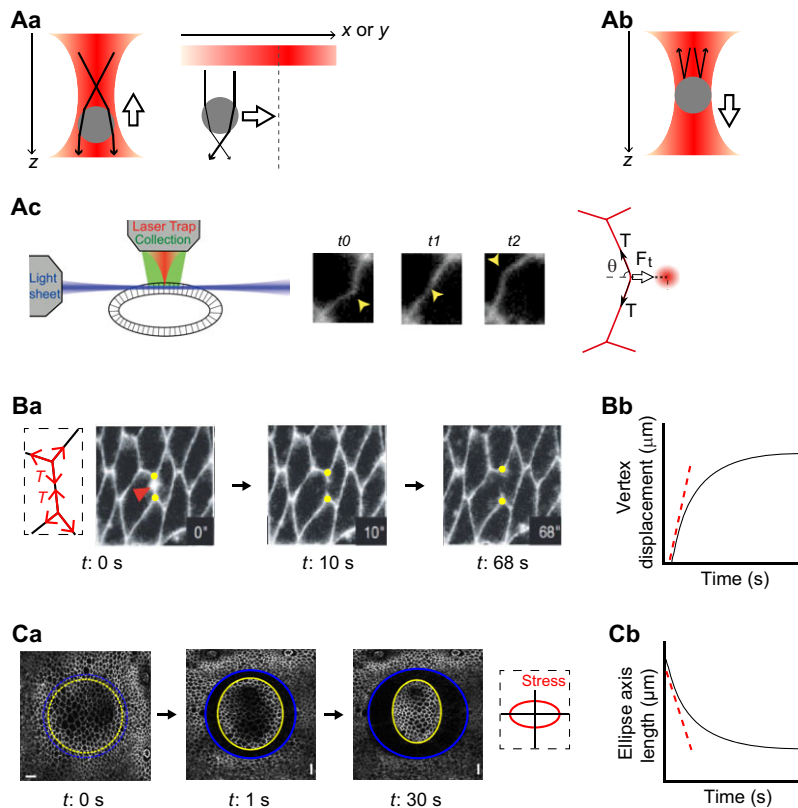
Fig. 2. Manipulation with light. (A) Optical tweezers. Principle of the optical trap. A transparent particle (with a higher refraction index than the surrounding medium) in a focused beam [red; color scale indicates the light intensity (I)] is subject to two forces: a gradient (Aa) and a scattering force (Ab). (Aa) The gradient force (F_{grad}; unfilled arrows) pulls the particle along the optical axis (z) and in the transverse plane (x, y), towards the highest intensity region, which is the beam focus (dashed line in the right panel). The black arrows indicate the refraction of light. (Ab) The scattering force (F_{scat}; unfilled arrow) pushes the particle away from the beam focus in the direction of incident light. The black arrows indicate the scattering of light. An effective optical trap occurs when F_{grad} dominates over F_{scat}. (Ac) Subcellular structures can also be trapped directly. Trapping a cell-cell interface and moving it (shown in three successive pictures ($t0$, $t1$ and $t2$) of the *Drosophila* embryonic ectoderm) can be used to determine tension (T) by considering the balance between T and the trapping force (F_t), according to the equation $F_t=2T\cos\theta$, where θ is the angle that the interface makes with respect to F_t. (B) Subcellular laser ablation. (Ba) Inset shows network of tensions (T) at $t=0$. Upon irradiation with a laser (red arrowhead), vertices of the manipulated cell-cell interface (yellow circles) move apart, indicating that a positive, contracting tension was acting at the cell-cell interface. (Bb) The vertex displacement is plotted against time. A linear fit (red dashed line) to the initial velocity of vertices (V_{init}) can be used to determine the ratio of the cell-cell interface tension (T) to the viscous drag, which resists the flow ($V_{init}\sim$tension/drag). (C) Tissue-scale laser ablation. (Ca) After severing a large circle of cells (cells placed between yellow and blue dashed lines), the wound opens either isotropically or anisotropically. Its internal margin (yellow line) and outer margin (blue line) take the shape of an ellipse, revealing the anisotropy of tissue stress before ablation, here stronger along the horizontal axis (as shown in the inset). (Cb) The ellipse (here the internal one) has two main axes, one large and one small, and the analysis is performed separately along each axis. The axis size is plotted against time. The initial rate of axis length decrease (V_{init}) measures the ratio of the tissue stress before ablation to the tissue viscosity, which resists deformation ($V_{init}\sim$stress/viscosity). Adapted with permission from: (Ac) Bambardekar et al. (2015), (Ba) Rauzi et al. (2008) and (Ca) Bonnet et al. (2012).

according to the equation $E=R_0^6/(R^6+R_0^6)$, where R_0 is the distance at which FRET efficiency is 50% (Fig. 3Ab). A spring of known stiffness, such as a defined polypeptide sequence, is genetically inserted between donor and acceptor (Meng et al., 2008; Grashoff et al., 2010). A force pulling on the molecule increases the spring length, thus reducing FRET efficiency. The FRET efficiency-force relationship is calibrated *in vitro*; typically, it probes from one to several pN (Grashoff et al., 2010; Fig. 3Ac). This technique relies on the assumption that molecular tension is the only cause of FRET change, which has to be tested using tensionless control constructs, e.g. lacking the N- or C-termini of the encoded proteins, under the same perturbations as their tension-sensing counterpart. In principle, this allows non-tension contributions to FRET changes, regardless of their origin, to be corrected for.

A major advantage of the method is that it could be applicable to any protein of interest as long as the tagged protein (containing the tension sensor) retains the localization and functions of the native protein. In addition, the method is, in principle, compatible with imaging of other proteins and/or structures, other force measurements, or any mechanical manipulation performed on a microscope stage. Within a very short time period (the time for image acquisition, typically around 100 ms), a map of molecular tensions (for the tagged molecule) in a tissue can be obtained *in vivo*: each pixel intensity results from the sum of FRET efficiencies of the molecules within this pixel. In cell culture, FRET has also been used to measure uniaxial compression (Paszek et al., 2014). More generally, fluorescent materials exhibit a variety of properties that could be dependent on other mechanical quantities, such as intracellular pressure (Gomez-Martinez et al., 2013; Watanabe et al., 2013), and thus could be used to develop new force probes.

One limitation of this method is its assumption that inserting a tension sensor module into a host protein does not change the efficiency-force relationship, and that the calibration *in vitro* remains valid *in vivo*. Another drawback is that only the amplitude of tension (not its orientation) within a molecule is measured; tension (molecule stretching) but not compression
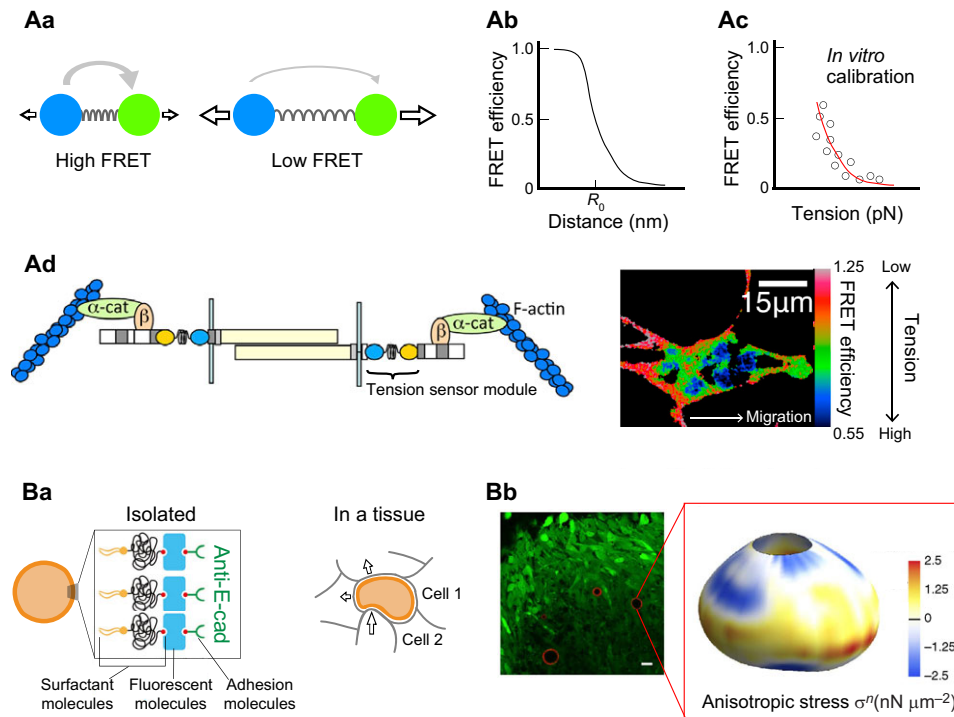
Fig. 3. Visual sensors. (A) FRET. (Aa) FRET tension sensor module consists of two fluorophores, a donor (blue) and an acceptor (green), linked with a spring of known stiffness, the length of which increases with pulling forces (arrows) acting on it. (Ab) Energy transfer efficiency (light gray arrows in Aa) sharply decreases with the distance between fluorophores. (Ac) The FRET efficiency-force relationship is experimentally calibrated *in vitro*. Red line indicates a fitting curve. (Ad) FRET tension sensor module inserted into DE-cadherin molecules can measure their tension. FRET efficiency (color bar) in border cells of *Drosophila* ovary is shown. (B) Liquid drop. (Ba) A liquid drop made of fluorocarbon oil (light orange) is coated by surfactant molecules, fluorescent molecules and adhesion molecules. The surface tension (γ) of an isolated drop is measured in solution (left panel). When the liquid drop is inserted between cells in a tissue (right panel), it is deformed by cellular forces (arrows). Image analysis determines the local mean curvature of the droplet surface (H), from which the anisotropic component of the normal stresses on the droplet (σ) can be determined according to the equation $\sigma = 2\gamma H$. (Bb) Liquid drops (red) injected between tooth mesenchymal cells (green). Scale bar: 20 μm. The values of the anisotropic stresses (color bar) are mapped onto the three-dimensional shape of the liquid drop (enlarged in inset). Adapted with permission from: (Ad) Cai et al. (2014) and (Ba, Bb) Campàs et al. (2014).

(molecule shortening) can be detected. Finally, the measurement fails when the force is too large (when the spring is entirely stretched or the FRET efficiency too low); molecular tensions might therefore be underestimated.

FRET tension sensors have been successfully applied to adhesion and cytoskeleton-related proteins in cell culture (Grashoff et al., 2010; Borghi et al., 2012; Conway et al., 2013) and have also been used in *in vivo* model systems. For example, in *C. elegans*, this approach revealed that tension in β-spectrin ensures the structural integrity of touch receptor neurons and supports efficient sensation of touch (Krieg et al., 2014). In the *Drosophila* ovary, FRET sensors were used to demonstrate that a difference in DE-cadherin (Shotgun) tension between the front and back of a migrating cell population underlies collective directional cell movement (Cai et al., 2014; Fig. 3Ad).

Liquid drops

In the absence of externally applied stresses, the principle that interfaces tend to be minimized owing to surface tension implies that a liquid drop will be spherical. When a drop is introduced between cells in a tissue, stresses exerted by neighboring cells or by the extracellular matrix counteract surface tension and deform the drop (Campàs et al., 2014; Fig. 3Ba). The drops are stress transducers, like the mechanical elements described in the 'Pushing' section above, yet they are incorporated into the tissue and are pushed and deformed within it. Confocal microscopy can be used to determine the three-dimensional drop shape, which enables inference of the anisotropic stresses locally

exerted on the drop (Fig. 3Ba). Provided that the drops are small enough compared with tissue size, they can be left in place for days without affecting normal embryonic development, and thus measure changes in stresses over a period of time.

Drops used in stress measurements should be fluorescently labeled, made of bio-compatible oil, cell-sized, and coated with ligands for cell adhesion receptors so that both tensile and compressive stresses can be measured (for details, see chapter 20 of Paluch, 2015). The drop size should remain below a limit (600 μm for fluorocarbon oil) to avoid deformation by gravity, and above a size (typically 10 μm in diameter) that would allow internalization by cells.

Drop contour curvatures can typically be measured with ±5% accuracy (depending on image resolution). The value of the interfacial tension of the drop can be tuned to enlarge the range of measurable stresses, from ~0.1 to 60 kPa. When the interfacial tension of the drop is lower, the drop deforms more for a given stress. The main limitation of this method is that the interfacial tension has to be known. This can be measured for the isolated drop before introduction into the tissue; the accuracy is around 20% for the minimal interfacial tensions used (~3 mN/m). However, this relies on the assumption that the interfacial tension remains constant and uniform when the drop, being introduced between cells, comes into contact with proteins that can adsorb on its surface. If the drop surface has been saturated beforehand with surfactants, which leave no space available for protein adsorption, such a hypothesis is reasonable but should be validated independently.

DEVELOPMENT

This recently developed method has been tested both in cultured aggregates of tooth mesenchymal and mammary epithelial cells and in living tissue explants, showing for example that the anisotropic stresses generated by mammary epithelial cells are dependent on myosin II activity (Campàs et al., 2014; Fig. 3Bb).

It is possible to conceive of a variation of this method that uses a soft bead made of polymers in a microfluidic setup. The advantage of this would be that bead stiffness might be more controlled and calibrated than the drop, it might be tunable in a larger range, and it might be compressible and thus able to measure the pressure or traction in the surrounding tissue. Alternatively, gel sensors can be external instead of internal to yield accurate tissue-scale force determinations. For example, embedding *Xenopus* embryo tissue in soft agarose gels of differing stiffness has shown that dorsal tissues undergoing convergent extension upregulate force production when embedded in a stiffer microenvironment (Zhou et al., 2015).

Non-mechanical observation techniques

Finally, we present purely visual methods (that do not involve mechanical probing the tissue in any way) for which live imaging yields simultaneous information over a whole region of a tissue plane. Birefringence uses an intrinsic optical response of the tissue to stress anisotropy, and force inference is based on cell-shape analysis.

Birefringence

Anisotropic spatial distribution of molecular and cellular forces results in tissue stress anisotropy. When an otherwise isotropic material is subject to an anisotropic stress, there is a difference between its refraction indices in the direction of larger versus smaller stress. This difference, called 'birefringence', is equal to the stress anisotropy multiplied by the so-called 'photo-elastic constant', c, which characterizes the material. In a tissue, an image of polarized light intensity transmitted perpendicularly to the tissue plane reveals the map of stress anisotropy within the tissue (Fig. 4Aa; Oldenbourg, 2005).

This optical property of tissues can thus act as an indirect stress probe, the sensitivity of which is determined by c. Within a tissue, c can be measured *in vitro* in an explant if birefringence measurements are combined with a micro-manipulation setup to apply stress.
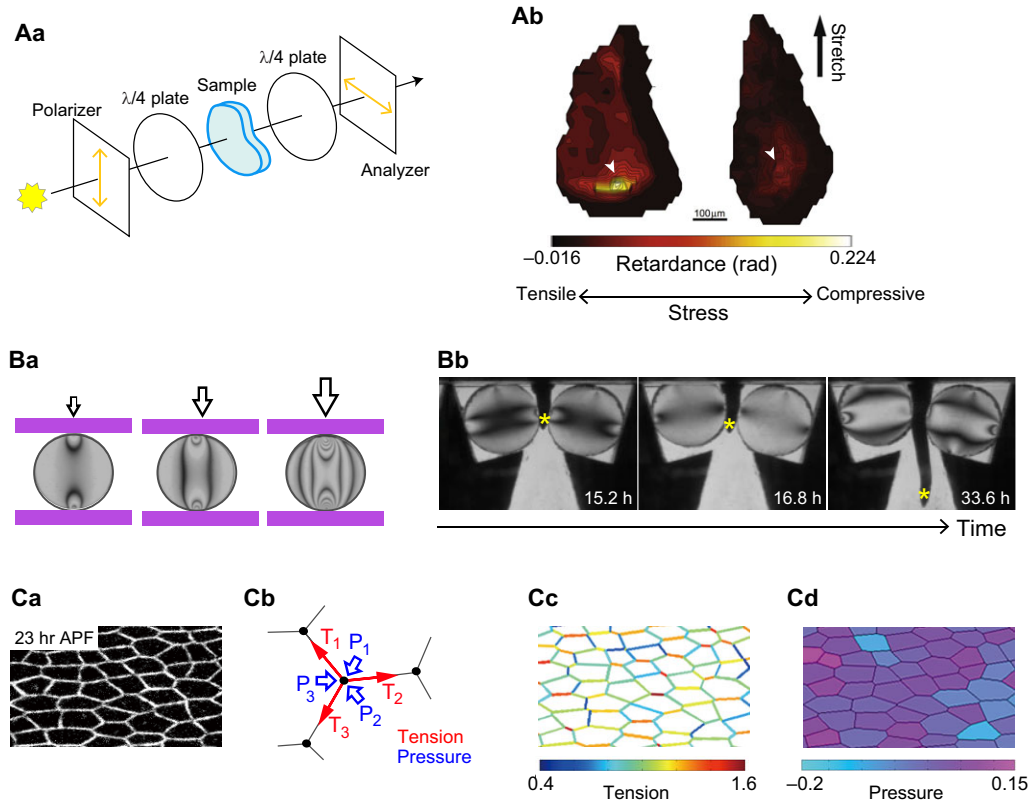

Fig. 4. Non-mechanical observation techniques. (A) Internal birefringence. (Aa) A tissue under anisotropic stress in axes 1 and 2 has different refractive indices in the directions of larger and smaller stresses (σ_1 and σ_2). This can be detected using polarized light. In the set-up shown, a sample of thickness d is placed between two sets of combined linear and quarter-wavelength polarizers and illuminated. The light beams polarized along axes 1 and 2 acquire a phase difference ('retardance') according to the refractive indices of the sample. Spatial variations of retardance therefore provide information on spatial stress anisotropies, according to the following equation: retardance~$c\,d\,(\sigma_1-\sigma_2)/\lambda$ (where c is the photo-elastic constant and λ is the wavelength of light). (Ab) Phase retardance maps (color bar) of control (left) and vertically stretched (right) *Drosophila* wing discs. Compressive stress builds up in the center of wing pouch (white arrowheads). Compression is released by tissue stretching. (B) External birefringence. (Ba) By changing the magnitude of forces applied on a calibrated birefringent disk, different fringe patterns are obtained. (Bb) Measurement of forces during the growth of a chickpea root. Fringe patterns are used to infer radial forces exerted by the root. Yellow asterisks label the root tip. (C) Force inference. (Ca) Input image of epithelial cell shapes, here in *Drosophila* pupal wing at 23 h after pupa formation (APF). (Cb) Image analysis yields cell shapes, vertex positions and connectivity; they are expressed in force-balance equations, which encompass the pattern geometry and reflect the balance of the set of cell-cell interface tensions (T) and differences of cell pressures (P) to be determined. (Cc) Solving these force-balance equations yields a map of cell-cell interface tensions, shown relative to an unknown constant, which is the average tension. (Cd) The inferred map of cell pressures has another unknown, an additive constant, which is the average pressure. Adapted with permission from: (A) Nienhaus et al. (2009), (B) Kolb et al. (2012), (C) Ishihara and Sugimura (2012).

An advantage of this method is that it is non-destructive and simple. A crude version can be implemented with any camera (and, where required, a microscope), and its space-time resolution is that of the camera. Several more elaborate methods have been developed (Oldenbourg, 2005) that can allow, for example, the stress directions to be determined. However, for birefringence measurements to be quantitative, the object studied should be flat (or the thickness profile known), transparent and homogeneous; the mechanical stresses must be within the two-dimensional plane; and c should be calibrated. This is straightforward in engineering science, but much more complicated *in vivo*, where this technique is used for relative measurements (with accuracy of up to ±10%). Moreover, *in vivo*, anisotropy can have additional causes other than stress, and birefringence quantifies changes in anisotropy presumed to be due to stress, rather than changes in stress itself.

Forces exerted by cells on a solid substrate down to 1 pN/μm² have been measured (Curtis et al., 2007). *In vivo*, in tissues such as *Drosophila* wing discs, c is of the order of 10^{-10} Pa⁻¹ and stresses of 10 kPa are detectable; birefringence has been used to measure changes in the distribution of stress during development (Nienhaus et al., 2009; Schluck and Aegerter, 2010; Fig. 4Ab). In this case, the stress distribution pattern supported theoretical models of wing disc growth, which hypothesize that the mutual feedback between cell proliferation and tissue stress could set tissue size and shape (Hufnagel et al., 2007; Aegerter-Wilmsen et al., 2007).

Alternatively, the birefringence of an external sensor (a known calibrated material such as plexiglass, agar gel or a commercial sensor) placed in contact with the tissue yields a pattern of optical fringes related to the stress field within the sensor (Fig. 4Ba). This yields semi-quantitative estimates of the force exerted by the tissue on the sensor (fully quantitative information is accessible in some simple cases). This technique is biocompatible, non-destructive and suitable for living systems larger than 1 mm that move and/or grow. For example, this method was used *in vivo* to quantify radial force of around 1 N during root growth in response to constraints (Fig. 4Bb), which provided insights into the mechanical interaction between the radial growth of roots and the porous or crack networks of soils and substrates (Kolb et al., 2012).

Force inference

In epithelial tissues at mechanical equilibrium where cell shapes are determined by the balance of contact forces between cells, such as cell-cell junction tensions and cell pressures, image observation yields information on these forces (Fig. 4C). For instance, if three cell-cell junctions with the same tension meet at a vertex, their respective angles should be equal by symmetry, and thus be 120° each. Reciprocally, any observed deviation from 120° enables estimation of the ratios of their tensions. As a junction has the same tension at both its ends, the tension ratios can be determined simultaneously across all junctions within a connected network (Stein and Gordon, 1982).

In simple cases, for example when cell junctions are straight and cell pressure differences negligible, it is straightforward to solve the relevant equations and determine the tension ratios (Chiou et al., 2012). However, where such assumptions cannot be applied, the number of unknown forces becomes larger than the number of equations, and more elaborate statistical methods may be required to calculate these forces (Ishihara and Sugimura, 2012; Ishihara et al., 2013). Adding visual measurements of cell-cell junction curvature, which is related to tensions and pressures, increases the number of equations above that of unknown forces, again enabling a direct resolution (Brodland et al., 2014; chapter 18 of Paluch, 2015).

The advantages of force inference are as follows. First, it is non-destructive, so that the dynamics of forces or stresses can be analyzed by live imaging in two or three dimensions. Second, the method is free from any assumption regarding the biophysical origin of tension and pressures. Third, it offers both single-cell resolution and a global stress map, which allows comparison of the inferred forces directly with the activity of adhesion or motor molecules, the cell-level dynamics, and the tissue-scale morphogenesis. Fourth, force inference lends itself well to various validations, for instance by looking at myosin distribution and cell junction ablation. Tests on a controlled pattern prepared using numerical simulations have shown its accuracy and robustness to added noise (Ishihara and Sugimura, 2012). It is also suitable for performing cross-validations against other measurement methods, as discussed further below.

However, there are also a number of drawbacks to this approach. First, it is a relative method: only ratios of tensions are measured, hence all tensions are determined relative to an unknown constant, which is the average tension. The situation is similar for pressures, as only pressure differences are measured, and the average pressure can be determined by another method (e.g. by contact manipulation). Second, it relies on cell-contour extraction, so determining tensions across a large number of cells requires an efficient image processing method, and a validation procedure to ensure that contour determination errors do not accumulate their effects (Brodland et al., 2014). Third, it measures only the 'junctional stress', i.e. the part of the stress that is transmitted through visible cell-cell junctions. This includes several forces generated within the bulk of a cell and transmitted to its neighbors through cell-cell junctions, but if other channels of stress transmission (e.g. through basal adhesion) exist, their contribution should be determined by another method.

Force inference has been applied *in vivo* to monolayered epithelia in *Drosophila* development (Sugimura and Ishihara, 2013). This study reported the distributions of tension, pressure and stress in the pupal wing (Fig. 4C), and showed that extrinsic stretching forces provide directional information for assignment of the orientation of cell rearrangements, leading to tissue elongation and hexagonal cell packing.

Relaxing the hypothesis that the tissue is in mechanical equilibrium, a dynamic version of force-inference named 'video force microscopy' uses temporal cell shape changes to infer forces. By analyzing movies of *Drosophila* embryogenesis where the non-muscle myosin is fluorescently labeled, such an approach has revealed the distribution of forces and the role of myosin in ventral furrow invagination (Brodland et al., 2010).

Conclusions

In the sections above, we have reviewed several force measurement techniques working at various scales *in vitro* or *in vivo*. They can provide some information on the sign, magnitude, orientation and/ or distribution of forces or stresses shaping tissues during development. We now discuss how these methods compare with each other and how they can be combined – both with each other, and with theoretical models. Finally, we provide a perspective on the future of this field.

Combinations and comparisons

Some of these methods are already established as standard tools in developmental biology, and we predict (and hope) that the others might also become standard soon. These techniques are diverse enough that they are complementary: for each system and biological question, a different technique will be the most suitable. Altogether,

they probe forces over a wide range of length and time scales. Importantly, most mechanical measurements are fast (from a few tens to thousands of seconds, see Table 1) compared with the timescales of morphogenetic events and are thus capable of following the temporal changes of forces during development.

In practice, the fields of application of these various methodologies are also diverse. Internal birefringence, optical tweezers and laser ablation require tissue transparency and apply mainly to thin or external tissues. Pipette aspiration, microplate and indentation can only be used on samples accessible to direct mechanical contact. Drops and beads require injection. FRET, force inference and drops rely on fluorescence imaging, and can be used in both two- and three-dimensional samples, provided the tissue depth does not render the signal probe undetectable.

Going forwards, it will be important to combine and apply these methods in a more integrated way, simultaneously using in the same tissue methods that measure different quantities or work at different scales. For instance, the combination of molecular-scale tension measurements (FRET sensors) with cell- and tissue-scale tension measurements or manipulations (e.g. with optical tweezers) may contribute to our description and understanding of the links between the scales of intracellular components, individual cells, groups of cells, and tissues. Moreover, measurements obtained using a small-scale probe can be gathered and presented over a much larger range. For instance, FRET-based molecular tension microscopy, force inference and birefringence are measured at the scales of molecules, cell junctions and groups of cells, respectively, but each can be suitably averaged over space to yield a tissue-scale map of some stress components. Finally, associating well-calibrated methods, such as contact manipulation, with force- or stress-mapping methods, such as FRET, birefringence or force inference, cumulate their advantages. For instance, if the value of one tension is determined by an absolute measurement method (e.g. by optical tweezers), this provides a value to the unknown constant in force inference, which hence becomes an absolute measurement too.

Pairwise comparisons of two methods that measure the same quantities at the same scale in the same place provide cross-validation so that results are more reliable and less dependent on assumptions. In *Drosophila* epithelial tissues, force inference has been successfully compared with birefringence (Ishihara and Sugimura, 2012) and with large-scale ablation anisotropy measurements (Ishihara et al., 2013). In the future, adequate systems could be designed to enable scale and penetration overlap, and calibration. Such systems could include cultured cell monolayers, reconstituted cell aggregates, or even foams. Establishing more *in vivo* systems that allow cross-validation will speed up the development of *in vivo* force or stress measurement methods and let a coherent picture emerge.

Links with modeling
Computational models based on mechanics are increasingly used in developmental biology (Keller, 2002). Whether using analytical equations or numerical simulations, they assist force and stress measurements in several respects (for reviews of models used in tissue mechanics, see Brodland, 2004; Anderson et al., 2007; Oates et al., 2009; Tlili et al., 2015). For instance, theoretical reasoning helped the conception and design of new force measurement techniques and experiments, such as tissue-scale laser ablation, drops, or optical tweezers without beads (Bonnet et al., 2012; Campàs et al., 2014; Bambardekar et al., 2015). Most methods reviewed here require models and assumptions to extract measurements of relevant parameters, if necessary through fits of

models to data, in particular for laser ablation and force inference experiments (Hutson et al., 2003; Farhadifar et al., 2007; Ishihara and Sugimura, 2012; Brodland et al., 2010, 2014). Numerical simulations provide benchmark data in controlled conditions, to validate an experimental measurement and test its sensitivity to a parameter or to errors (Landsberg et al., 2009; Ishihara et al., 2013; Brodland et al., 2014; Bambardekar et al., 2015). Finally, comparing experiments with analytical models or numerical simulations enables us to refine the interpretation of experimental results and extract from them more information, such as material properties, or quantities that are not directly accessible to experiments (Farhadifar et al., 2007; Krieg et al., 2008; Rauzi et al., 2008; Mayer et al., 2010; Bonnet et al., 2012; Maître et al., 2012; Sugimura and Ishihara, 2013; Forouzesh et al., 2013).

Although models are important for interpreting force and stress measurements, the opposite is true as well. Most models of tissue mechanics require some data on the distribution of forces. Quantitative measurements should enable not only the reduction in the number of unknown parameters, but also allow us to make experiment-based hypotheses and test falsifiable predictions arising from different models. This step is essential for developing predictive models of tissue mechanics, in an attempt to explain how cell-level changes (deformation, growth, mitosis, migration, neighbor swapping and apoptosis) determine, through mechanical interactions, the final shape and size of a tissue (Tlili et al., 2015).

Future directions
Historically, for practical and conceptual reasons, morphogenetic movements have typically been studied separately one from another, even though they may be occurring simultaneously within a developing organism. Now, with force and stresses measurements along with new imaging approaches, we expect a more integrated understanding of the interactions within and between tissues that determine their shape and movements. The equipment and know-how required for force or stress measurements are increasingly available in biophysics and biology laboratories, and are beginning to be applied across a large variety of developmental models, including mammals.

Force and stress measurements will be crucial for unraveling how the tissue mechanical properties are related one to another, from the molecular scale to the scale of cells, tissues and whole organisms, and from millisecond to hour timescales. It is likely that they will foster our understanding of emergent properties of tissues, such as the simultaneously solid-like and fluid-like mechanical behaviors of tissues at developmental timescales. This dual mechanical behavior arises from the relatively fast dynamics of cytoskeletal and adhesive structures, and cell mechanical activity generated by molecular motors, which generate and transmit forces. We also expect that the combination of mechanical measurements with the fast-growing optogenetic tools (Tischer and Weiner, 2014) will unveil important connections between mechanics and biochemical signaling; obtaining a coherent picture should illuminate the coupling between biochemical and mechanical regulations in tissues.

References

Addae-Mensah, K. A. and Wikswo, J. P. (2008). Measurement techniques for cellular biomechanics in vitro. *Exp. Biol. Med.* **233**, 792-809.

Aegerter-Wilmsen, T., Aegerter, C. M., Hafen, E. and Basler, K. (2007). Model for the regulation of size in the wing imaginal disc of *Drosophila*. *Mech. Dev.* **124**, 318-326.

Anderson, A. R. A., Chaplain, M. A. J. and Rejniak, K. A. (ed.) (2007). *Single Cell Based Models in Biology and Medicine*. Basel: Birkhäuser.

Bambardekar, K., Clément, R., Blanc, O., Chardès, C. and Lenne, P.-F. (2015). Direct laser manipulation reveals the mechanics of cell contacts *in vivo*. *Proc. Natl. Acad. Sci. USA* **112**, 1416-1421.

Beauzamy, L., Nakayama, N. and Boudaoud, A. (2014). Flowers under pressure: ins and outs of turgor regulation in development. *Ann. Bot.* **114**, 1517-1533.

Beauzamy, L., Derr, J. and Boudaoud, A. (2015). Quantifying hydrostatic pressure in plant cells by using indentation with an atomic force microscope. *Biophys. J.* **108**, 2448-2456.

Behrndt, M., Salbreux, G., Campinho, P., Hauschild, R., Oswald, F., Roensch, J., Grill, S. W. and Heisenberg, C.-P. (2012). Forces driving epithelial spreading in *zebrafish* gastrulation. *Science* **338**, 257-260.

Beloussov, L. V., Dorfman, J. G. and Cherdantzev, V. G. (1975). Mechanical stresses and morphological patterns in amphibian embryos. *J. Embryol. Exp. Morphol.* **34**, 559-574.

Bertet, C., Sulak, L. and Lecuit, T. (2004). Myosin-dependent junction remodelling controls planar cell intercalation and axis elongation. *Nature* **429**, 667-671.

Bonnet, I., Marcq, P., Bosveld, F., Fetler, L., Bellaïche, Y. and Graner, F. (2012). Mechanical state, material properties and continuous description of an epithelial tissue. *J. R. Soc. Interface* **9**, 2614-2623.

Borghi, N., Sorokina, M., Shcherbakova, O. G., Weis, W. I., Pruitt, B. L., Nelson, W. J. and Dunn, A. R. (2012). E-cadherin is under constitutive actomyosin-generated tension that is increased at cell-cell contacts upon externally applied stretch. *Proc. Natl. Acad. Sci. USA* **109**, 12568-12573.

Brodland, G. W. (2004). Computational modeling of cell sorting, tissue engulfment and related phenomena: a review. *Appl. Mech. Rev.* **57**, 47-76.

Brodland, G. W., Conte, V., Cranston, P. G., Veldhuis, J., Narasimhan, S., Hutson, M. S., Jacinto, A., Ulrich, F., Baum, B. and Miodownik, M. (2010). Video force microscopy reveals the mechanics of ventral furrow invagination in *Drosophila*. *Proc. Natl. Acad. Sci. USA* **107**, 22111-22116.

Brodland, G. W., Veldhuis, J. H., Kim, S., Perrone, M., Mashburn, D. and Hutson, M. S. (2014). CellFIT: a cellular force-inference toolkit using curvilinear cell boundaries. *PLoS ONE* **9**, e99116.

Cai, D., Chen, S.-C., Prasad, M., He, L., Wang, X., Choesmel-Cadamuro, V., Sawyer, J. K., Danuser, G. and Montell, D. J. (2014). Mechanical feedback through E-cadherin promotes direction sensing during collective cell migration. *Cell* **157**, 1146-1159.

Campàs, O., Mammoto, T., Hasso, S., Sperling, R. A., O'Connell, D., Bischof, A. G., Maas, R., Weitz, D. A., Mahadevan, L. and Ingber, D. E. (2014). Quantifying cell-generated mechanical forces within living embryonic tissues. *Nat. Methods* **11**, 183-189.

Campinho, P., Behrndt, M., Ranft, J., Risler, T., Minc, N. and Heisenberg, C.-P. (2013). Tension-oriented cell divisions limit anisotropic tissue tension in epithelial spreading during zebrafish epiboly. *Nat. Cell Biol.* **15**, 1405-1414.

Chiou, K. K., Hufnagel, L. and Shraiman, B. I. (2012). Mechanical stress inference for two dimensional cell arrays. *PLoS Comput. Biol.* **8**, e1002512.

Conway, D. E., Breckenridge, M. T., Hinde, E., Gratton, E., Chen, C. S. and Schwartz, M. A. (2013). Fluid shear stress on endothelial cells modulates mechanical tension across VE-cadherin and PECAM-1. *Curr. Biol.* **23**, 1024-1030.

Curtis, A., Sokolikova-Csaderova, L. and Aitchison, G. (2007). Measuring cell forces by a photoelastic method. *Biophys. J.* **92**, 2255-2261.

Davidson, L. and Keller, R. (2007). Measuring mechanical properties of embryos and embryonic tissues. *Methods Cell Biol.* **83**, 425-439.

Davidson, L., von Dassow, M. and Zhou, J. (2009). Multi-scale mechanics from molecules to morphogenesis. *Int. J. Biochem. Cell Biol.* **41**, 2147-2162.

Davis, G. S. (1984). Migration-directing liquid properties of embryonic amphibian tissues. *Am. Zool.* **24**, 649-655.

Etournay, R., Popović, M., Merkel, M., Nandi, A., Blasse, C., Aigouy, B., Brandl, H., Myers, G., Salbreux, G., Jülicher, F. et al. (2015). Interplay of cell dynamics and epithelial tension during morphogenesis of the *Drosophila* pupal wing. *Elife* **4**, e07090.

Evans, E. and Yeung, A. (1989). Apparent viscosity and cortical tension of blood granulocytes determined by micropipet aspiration. *Biophys. J.* **56**, 151-160.

Farge, E. (2003). Mechanical induction of Twist in the *Drosophila* foregut/stomodeal primordium. *Curr. Biol.* **13**, 1365-1377.

Farhadifar, R., Röper, J.-C., Aigouy, B., Eaton, S. and Jülicher, F. (2007). The influence of cell mechanics, cell-cell interactions, and proliferation on epithelial packing. *Curr. Biol.* **17**, 2095-2104.

Fernández-Sánchez, M. E., Barbier, S., Whitehead, J., Béalle, G., Michel, A., Latorre-Ossa, H., Rey, C., Fouassier, L., Claperon, A., Brullé, L. et al. (2015). Mechanical induction of the tumorigenic β-catenin pathway by tumour growth pressure. *Nature* **523**, 92-95.

Forouzesh, E., Goel, A., Mackenzie, S. A. and Turner, J. A. (2013). In vivo extraction of Arabidopsis cell turgor pressure using nanoindentation in conjunction with finite element modeling. *Plant J.* **73**, 509-520.

Foty, R. A., Forgacs, G., Pfleger, C. M. and Steinberg, M. S. (1994). Liquid properties of embryonic tissues: measurement of interfacial tensions. *Phys. Rev. Lett.* **72**, 2298-2301.

Foty, R. A., Pfleger, C. M., Forgacs, G. and Steinberg, M. S. (1996). Surface tensions of embryonic tissues predict their mutual envelopment behavior. *Development* **122**, 1611-1620.

Fung, Y. C. (1993). *Biomechanics: Mechanical Properties of Living Tissues*. Berlin: Springer.

Gayrard, C. and Borghi, N. (2015). FRET-based molecular tension microscopy. *Methods*, doi: 10.1016/j.ymeth.2015.07.010.

Gomez-Martinez, R., Hernandez-Pinto, A. M., Duch, M., Vazquez, P., Zinoviev, K., de la Rosa, E. J., Esteve, J., Suarez, T. and Plaza, J. A. (2013). Silicon chips detect intracellular pressure changes in living cells. *Nat. Nanotechnol.* **8**, 517-521.

Grashoff, C., Hoffman, B. D., Brenner, M. D., Zhou, R., Parsons, M., Yang, M. T., McLean, M. A., Sligar, S. G., Chen, C. S., Ha, T. et al. (2010). Measuring mechanical tension across vinculin reveals regulation of focal adhesion dynamics. *Nature* **466**, 263-266.

Guevorkian, K., Colbert, M.-J., Durth, M., Dufour, S. and Brochard-Wyart, F. (2010). Aspiration of biological viscoelastic drops. *Phys. Rev. Lett.* **104**, 218101.

Guillot, C. and Lecuit, T. (2013). Mechanics of epithelial tissue homeostasis and morphogenesis. *Science* **340**, 1185-1189.

Heisenberg, C.-P. and Bellaïche, Y. (2013). Forces in tissue morphogenesis and patterning. *Cell* **153**, 948-962.

Hufnagel, L., Teleman, A. A., Rouault, H., Cohen, S. M. and Shraiman, B. I. (2007). On the mechanism of wing size determination in fly development. *Proc. Natl. Acad. Sci. USA* **104**, 3835-3840.

Hutson, M. S., Tokutake, Y., Chang, M.-S., Bloor, J. W., Venakides, S., Kiehart, D. P. and Edwards, G. S. (2003). Forces for morphogenesis investigated with laser microsurgery and quantitative modeling. *Science* **300**, 145-149.

Ishihara, S. and Sugimura, K. (2012). Bayesian inference of force dynamics during morphogenesis. *J. Theor. Biol.* **313**, 201-211.

Ishihara, S., Sugimura, K., Cox, S. J., Bonnet, I., Bellaïche, Y. and Graner, F. (2013). Comparative study of non-invasive force and stress inference methods in tissue. *Eur. Phys. J. E* **36**, 45.

Kahn, J., Shwartz, Y., Blitz, E., Krief, S., Sharir, A., Breitel, D. A., Rattenbach, R., Relaix, F., Maire, P., Rountree, R. B. et al. (2009). Muscle contraction is necessary to maintain joint progenitor cell fate. *Dev. Cell* **16**, 734-743.

Keller, E. F. (2002). *Making Sense of Life: Explaining Biological Development with Models, Metaphors, and Machines*. Harvard: Harvard University Press.

Kiehart, D. P., Galbraith, C. G., Edwards, K. A., Rickoll, W. L. and Montague, R. A. (2000). Multiple forces contribute to cell sheet morphogenesis for dorsal closure in *Drosophila*. *J. Cell Biol.* **149**, 471-490.

Koehl, M. A. R. (1990). Biomechanical approaches to morphogenesis. *Semin. Dev. Biol.* **1**, 367-378.

Kolb, E., Hartmann, C. and Genet, P. (2012). Radial force development during root growth measured by photoelasticity. *Plant Soil* **360**, 19-35.

Kollmannsberger, P. and Fabry, B. (2011). Linear and nonlinear rheology of living cells. *Annu. Rev. Mater. Res.* **41**, 75-97.

Krieg, M., Arboleda-Estudillo, Y., Puech, P.-H., Käfer, J., Graner, F., Müller, D. J. and Heisenberg, C.-P. (2008). Tensile forces govern germ-layer organization in zebrafish. *Nat. Cell Biol.* **10**, 429-436.

Krieg, M., Dunn, A. R. and Goodman, M. B. (2014). Mechanical control of the sense of touch by beta-spectrin. *Nat. Cell Biol.* **16**, 224-233.

Labouesse, M. (ed.). (2011). Forces and tension in development. *Curr. Top. Dev. Biol.* **95**, 2-270.

Landsberg, K. P., Farhadifar, R., Ranft, J., Umetsu, D., Widmann, T. J., Bittig, T., Said, A., Jülicher, F. and Dahmann, C. (2009). Increased cell bond tension governs cell sorting at the *Drosophila* anteroposterior compartment boundary. *Curr. Biol.* **19**, 1950-1955.

Larson, S. M., Lee, H. J., Hung, P.-H., Matthews, L. M., Robinson, D. N. and Evans, J. P. (2010). Cortical mechanics and meiosis II completion in mammalian oocytes are mediated by myosin-II and Ezrin-Radixin-Moesin (ERM) proteins. *Mol. Biol. Cell* **21**, 3182-3192.

Lecuit, T., Lenne, P.-F. and Munro, E. (2011). Force generation, transmission, and integration during cell and tissue morphogenesis. *Annu. Rev. Cell Dev. Biol.* **27**, 157-184.

Lomakina, E. B., Spillmann, C. M., King, M. R. and Waugh, R. E. (2004). Rheological analysis and measurement of neutrophil indentation. *Biophys. J* **87**, 4246-4258.

Ma, X., Lynch, H. E., Scully, P. C. and Hutson, M. S. (2009). Probing embryonic tissue mechanics with laser hole drilling. *Phys. Biol.* **6**, 036004.

Maître, J.-L., Berthoumieux, H., Krens, S. F. G., Salbreux, G., Jülicher, F., Paluch, E. and Heisenberg, C.-P. (2012). Adhesion functions in cell sorting by mechanically coupling the cortices of adhering cells. *Science* **338**, 253-256.

Maître, J.-L., Niwayama, R., Turlier, H., Nédélec, F. and Hiragi, T. (2015). Pulsatile cell-autonomous contractility drives compaction in the mouse embryo. *Nat. Cell Biol.* **17**, 849-855.

Mammoto, A., Mammoto, T. and Ingber, D. E. (2012). Mechanosensitive mechanisms in transcriptional regulation. *J. Cell Sci.* **125**, 3061-3073.

Mayer, M., Depken, M., Bois, J. S., Jülicher, F. and Grill, S. W. (2010). Anisotropies in cortical tension reveal the physical basis of polarizing cortical flows. *Nature* **467**, 617-621.

Mazuel, F., Reffay, M., Du, V., Bacri, J.-C., Rieu, J.-P. and Wilhelm, C. (2015). Magnetic flattening of stem-cell spheroids indicates a size-dependent elastocapillary transition. *Phys. Rev. Lett.* **114**, 098105.

Meng, F., Suchyna, T. M. and Sachs, F. (2008). A fluorescence energy transfer-based mechanical stress sensor for specific proteins in situ. *FEBS J.* **275**, 3072-3087.

Mgharbel, A., Delanoë-Ayari, H. and Rieu, J.-P. (2009). Measuring accurately liquid and tissue surface tension with a compression plate tensiometer. *HFSP J.* **3**, 213-221.

Mitchison, J. M. and Swann, M. M. (1954). The mechanical properties of the cell surface. *J. Exp. Biol.* **31**, Part I: 443-460; Part II: 461-472.

Miyawaki, A. (2011). Development of probes for cellular functions using fluorescent proteins and fluorescence resonance energy transfer. *Annu. Rev. Biochem.* **80**, 357-373.

Nienhaus, U., Aegerter-Wilmsen, T. and Aegerter, C. M. (2009). Determination of mechanical stress distribution in *Drosophila* wing discs using photoelasticity. *Mech. Dev.* **126**, 942-949.

Norotte, C., Marga, F., Neagu, A., Kosztin, I. and Forgacs, G. (2008). Experimental evaluation of apparent tissue surface tension based on the exact solution of the Laplace equation. *Europhys. Lett.* **81**, 46003.

Oates, A. C., Gorfinkiel, N., González-Gaitán, M. and Heisenberg, C.-P. (2009). Quantitative approaches in developmental biology. *Nat. Rev. Genet.* **10**, 517-530.

Oldenbourg, R. (2005). Polarization microscopy with the LC-PolScope. In *Live Cell Imaging: A Laboratory Manual* (ed. R. D. Goldman and D. L. Spector), pp. 205-237. Cold Spring Harbor, NY: Cold Spring Harbor Laboratory Press.

Paluch, E. K. (ed.) (2015). Biophysical methods in cell biology. *Meth. Cell Biol.* **125**, 1-488.

Paszek, M. J., DuFort, C. C., Rossier, O., Bainer, R., Mouw, J. K., Godula, K., Hudak, J. E., Lakins, J. N., Wijekoon, A. C., Cassereau, L. et al. (2014). The cancer glycocalyx mechanically primes integrin-mediated growth and survival. *Nature* **511**, 319-325.

Porazinski, S., Wang, H., Asaoka, Y., Behrndt, M., Miyamoto, T., Morita, H., Hata, S., Sasaki, T., Krens, S. F. G., Osada, Y. et al. (2015). YAP is essential for tissue tension to ensure vertebrate 3D body shape. *Nature* **521**, 217-221.

Rauzi, M., Verant, P., Lecuit, T. and Lenne, P.-F. (2008). Nature and anisotropy of cortical forces orienting *Drosophila* tissue morphogenesis. *Nat. Cell Biol.* **10**, 1401-1410.

Sampathkumar, A., Yan, A., Krupinski, P. and Meyerowitz, E. M. (2014). Physical forces regulate plant development and morphogenesis. *Curr. Biol.* **24**, R475-R483.

Savin, T., Kurpios, N. A., Shyer, A. E., Florescu, P., Liang, H., Mahadevan, L. and Tabin, C. J. (2011). On the growth and form of the gut. *Nature* **476**, 57-62.

Schluck, T. and Aegerter, C. M. (2010). Photo-elastic properties of the wing imaginal disc of *Drosophila*. *Eur. Phys. J. E* **33**, 111-115.

Stein, M. B. and Gordon, R. (1982). Epithelia as bubble rafts: a new method for analysis of cell shape and intercellular adhesion in embryonic and other epithelia. *J. Theor. Biol.* **97**, 625-639.

Sugimura, K. and Ishihara, S. (2013). The mechanical anisotropy in a tissue promotes ordering in hexagonal cell packing. *Development* **140**, 4091-4101.

Svoboda, K. and Block, S. M. (1994). Biological applications of optical forces. *Annu. Rev. Biophys. Biomol. Struct.* **23**, 247-285.

Tanase, M., Biais, N. and Sheetz, M. (2007). Magnetic tweezers in cell biology. *Methods Cell Biol.* **83**, 473-493.

Tinevez, J.-Y., Schulze, U., Salbreux, G., Roensch, J., Joanny, J.-F. and Paluch, E. (2009). Role of cortical tension in bleb growth. *Proc. Natl. Acad. Sci. USA* **106**, 18581-18586.

Tischer, D. and Weiner, O. D. (2014). Illuminating cell signalling with optogenetic tools. *Nat. Rev. Mol. Cell Biol.* **15**, 551-558.

Tlili, S., Gay, C., Graner, F., Marcq, P., Molino, F. and Saramito, P. (2015). Mechanical formalism for tissue dynamics. *Eur. Phys. J. E* **38**, 33-63.

Trejo, M., Douarche, C., Bailleux, V., Poulard, C., Mariot, S., Regeard, C. and Raspaud, E. (2013). Elasticity and wrinkled morphology of Bacillus Subtilis pellicles. *Proc. Natl. Acad. Sci. USA* **110**, 2011-2016.

Watanabe, T. M., Imada, K., Yoshizawa, K., Nishiyama, M., Kato, C., Abe, F., Morikawa, T. J., Kinoshita, M., Fujita, H. and Yanagida, T. (2013). Glycine insertion makes yellow fluorescent protein sensitive to hydrostatic pressure. *PLoS ONE* **8**, e73212.

Young, P. E., Pesacreta, T. C. and Kiehart, D. P. (1991). Dynamic changes in the distribution of cytoplasmic myosin during *Drosophila* embryogenesis. *Development* **111**, 1-14.

Zhou, J., Pal, S., Maiti, S. and Davidson, L. A. (2015). Force production and mechanical accommodation during convergent extension. *Development* **142**, 692-701.

DEVELOPMENT